Bi nanowires modified by 400 keV and 1 MeV Au ions

Cite as: AIP Advances **8**, 125103 (2018); https://doi.org/10.1063/1.5063463
Submitted: 27 September 2018 • Accepted: 23 November 2018 • Published Online: 04 December 2018

D. B. Guerra, S. Müller, M. P. Oliveira, et al.

Bi nanowires modified by 400 keV and 1 MeV Au ions

D. B. Guerra,[1] S. Müller,[1] M. P. Oliveira,[1] P. F. P. Fichtner,[2] and R. M. Papaléo[1]
[1]*Interdisciplinary Center of Nanoscience and Micro-Nanotechnology, School of Sciences, Pontifical Catholic University of Rio Grande do Sul, Porto Alegre, Brazil*
[2]*Institute of Physics, Federal University of Rio Grande do Sul, Porto Alegre, Brazil*

(Received 27 September 2018; accepted 23 November 2018; published online 4 December 2018)

We report on the modification of the structure and morphology of Bi nanowires of two different diameters (80 or 130 nm) exposed to beams of 400 keV and 1 MeV Au^+ until complete wire degradation. For fluences up to ~1 ion/nm^2, the main effect was a slight roughening of the originally smooth surface and the appearance of a damaged zone at the wire edges. After an exposure to ~2 ions/nm^2, shallow (~5-7 nm deep) but wide (up to 120nm) depressions are seen, giving the wires a "wavy" morphology. At the largest fluence tested (10 ions/nm^2), the thickest nanowires present an amorphized structure containing an embedded dispersion of small spherical metallic crystallites, while the thinner wires collapse into large (~50nm) nanoparticles composed of a crystalline core surrounded by a disordered oxidized shell. The observed morphologic modifications are discussed considering sputtering and radiation induced surface diffusion effects.
https://doi.org/10.1063/1.5063463

I. INTRODUCTION

Nanowires (NWs) grown from metals and semiconductor materials are considered to be of great importance in future nanotechnology applications. Among the great variety of materials, bismuth nanowires stands out for their unique transport properties, such as long mean free path and high mobility of charge carriers, which are essential in the development of modern microelectronics and thermoelectric devices.[1–4] Bismuth is an interesting material in the form of a nanowire, because quantum effects are expected in relatively large diameters.[5] Doping of nanowires may significantly improve their physical properties and further expands their applications. This can be achieved by introducing impurities during the growth, by thermal diffusion, or by ion implantation.[6–8] Ion implantation allows the control of the doping level with high precision,[8] and because it is a non-equilibrium process dopant concentrations beyond the standard limits of solubility can be achieved.[9,10] Besides, defect introduced by irradiation process may also modify the original wire properties and affect thermal and electrical properties of the wires independently.[2]

Radiation effects, however, may also be detrimental to the properties and performance of nanowires. For high-Z beams, sputtering is strong, leading to pronounced erosion of the original nanostructure, or excessive damage to the crystal structure.[11–13] In addition, the formation of vacancies and interstitials by ion irradiation may cause compressive and tensile stress in nanowires, leading to their bending.[14–16] Concerning irradiated single-crystalline bismuth nanowires, previous studies using proton beams with energies from 17.2 up to 40 MeV and low fluences[2,17] demonstrated the formation of grain boundaries and local amorphization, and a considerable reduction in the electrical and thermal conductivities of the nanowires. To the best of our knowledge, there are so far no reports of irradiation effects in Bi NW with ions heavier than H. For doping of Bi, halogen or metal atoms such as Br, Cu, Ag, Au are the most suitable elements.[18] For such ions, the implantation process is expected to introduce much more severe damage effects, due to the higher levels of deposited energy per ion and denser collision cascades. In this paper, we report on the

irradiation effects of 400 keV and 1 MeV Au beams on polycrystalline bismuth nanowires with diameters of 80 and 130 nm grown electrochemically in etched ion track templates. The changes in the morphology and structure of the wires were investigated until their complete destruction into nanoparticles.

II. MATERIAL AND METHODS

A. Sample preparation

Ion-track membranes were prepared by irradiation of polycarbonate (PC) foils (Makrofol, Bayer) with Au and U ions (energy, 5.9 and 11.1 MeV/u; fluence, 5×10^9 ions/cm^2) at the linear accelerator (UNILAC) at the GSI Helmholtz Centre for Heavy Ion Research. The foils were chemically etched in 6 mol/L NaOH solution to form cylindrical nanopores with mean diameters of 80 and 130 nm, depending on the chosen etching time. Subsequently, a thin Au layer with a thickness of 50 nm was deposited onto one side of the membranes to act as the cathode electrode for the electrochemical synthesis. Nanowire arrays were grown potentiostatically with a Gamry potentiostat in a two-electrode cell with a Pt counter electrode and a saturated calomel reference electrode (SCE). A Bi-rich electrolyte was prepared with bismuth trichloride ($BiCl_3$) and tartaric acid, as stated in Ref. 18. A constant voltage of 0 mV vs SCE was applied at 50 °C. The resulting nanowires have mean diameters (D_{NW}) of 80nm and 130nm, similar to the template matrix pores. In order to characterize and irradiate the nanowires, the PC template was dissolved using dichloromethane (CH_2Cl_2) and the nanowires were transferred to a TEM grid.

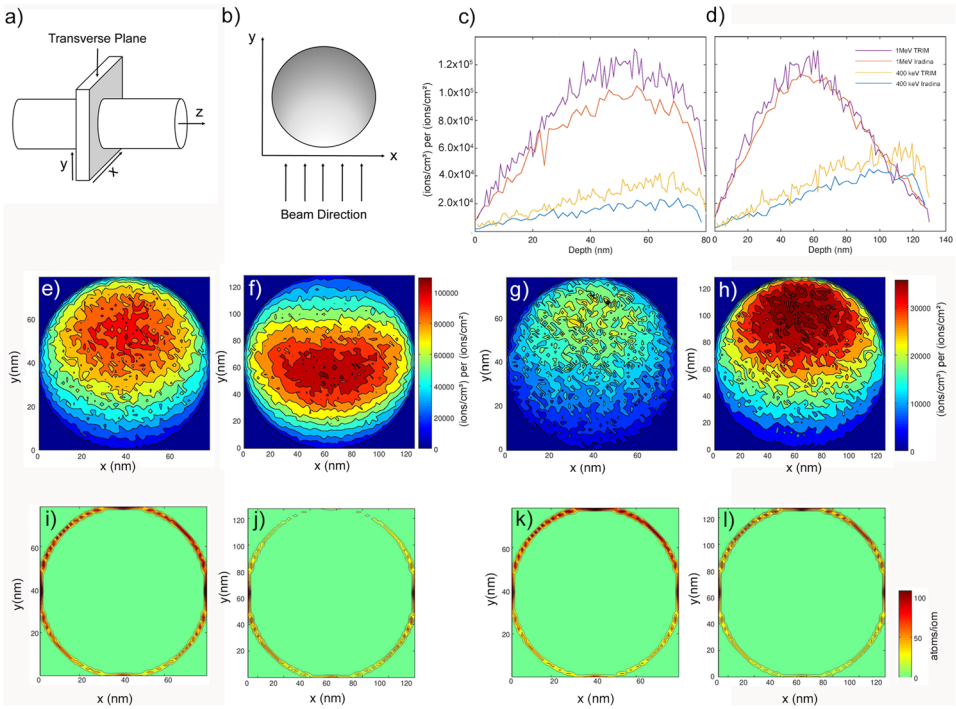

FIG. 1. MC simulation of the implantation of 400 keV and 1 MeV ions into Bi NWs. a) Schematics of the simulation geometry in Iradina. A transversal section of the nanowire (xy plane) is simulated with periodic boundary conditions applied along the NW axis (z-direction). b) The ions impinge on the wire along the y-direction at random positions across the x-axis. In the case of SRIM, flat layers of Bi were used instead of the wire. c) SRIM and Iradina 1D implantation profiles of 400 keV and 1 MeV Au ions incident on 80nm Bi NW or thin films. d) Similar to c) but for 130nm thick NW or thin films. e)-h) Two dimensional Iradina implantation profiles of 400 keV Au ions in e) 80 nm and f) 130 nm Bi nanowires, and of 1 MeV Au ions in g) 80 nm and h) 130 nm Bi NW. i)-l) Two dimensional Iradina sputtering profiles of 400 keV Au ions in i) 80 nm and j) 130 nm Bi nanowires, and of 1 MeV Au ions in k) 80 nm and l) 130 nm Bi NW.

B. Irradiation conditions and simulations

The SRIM-2013 software[19] was used to simulate the penetration and defect creation of Au beams of different energies in Bi thin films of thicknesses equivalent to the wire diameters. SRIM, however, cannot take into account the geometry and lateral limitations of a nanowire. Therefore *Iradina* (Ion Range and Damage in Nanostructures)[20,21] was also used to evaluate the irradiation parameters and implantation profiles into the nanowires. Both softwares are based on Monte Carlo simulations that rely on the binary collision approximation.[14] *Iradina* models the nanowires as a thin disk with periodic boundary conditions applied along the nanowire axis (z-direction). Thus, the simulation implies translational symmetry along the nanowire axis and infinite length.[21] This is a good approximation because the length of a real nanowire is around 100 times greater than its diameter. The simulations were carried out using the nanowire version of Iradina (Iradina_nw 1.0.5), according to the scheme shown in Fig. 1. The sensitive volume is divided into 50x50x1 cells. Each cell had a size (x,y,z) of 1.6×1.6×10 nm^3 for the 80nm wires and 2.6×2.6×10 nm^3 for the 130 nm wires. Thus, the total lateral size of the cell grid is equal to the wire diameter. The object is irradiated by 10^6 incident ions at right angles to the long axis of the wire and with random entry positions distributed over the x-axis. In order to compare with the output values obtained with SRIM, runs with a thin film geometry were also simulated in Iradina.[22] The values of the surface binding energy (2.17 eV), lattice binding energy (3 eV) and displacement energy (25 eV) used were the defaults values found in SRIM tables.

The irradiations were performed using a Tandetron 3 MV accelerator and a 500 kV ion implanter both from HVEE (The Netherlands).[23] The nanowires were irradiated directly on TEM grids in a vacuum chamber (~2x10^{-6} torr) at room temperature, with the beam direction perpendicular to the long axis of the wires. The samples were exposed to 400 keV and 1 MeV Au beams with a current density of 50 nA/cm^2 up to fluences of 1x10^{14}, 2x10^{14} and 1x10^{15} ions/cm^2 or 1, 2, and 10 ions/nm^2, respectively. The different stages of the degradation process were evaluated by scanning electron microscopy (FEI Inspect F50)[23] and transmission electron microscopy (TEM), using a JEOL JEM 2010 and a FEI Tecnai G2.[24]

III. RESULTS

A. Simulations

The fraction of transmitted ions (T %), the energy loss, the sputtering yield and other parameters extracted from the Monte Carlo simulations are shown in Table I. The total entrance dE/dx is only ~10% larger for the 1 MeV Au beam, essentially due to the higher electronic stopping. Typical sizes of collision cascades induced by a 400 keV or a 1 MeV Au simulated in SRIM are similar (~40 nm and ~47 nm, respectively), with a single primary ion displacing on average more than 10^4 atoms. The Bi recoil distribution peaks at a depth of ~40nm for the 400keV Au and has a FWHM close to 80 nm. For the 1MeV Au beam the recoil depth distribution is much broader (FWHM ~ 150 nm) with a wide peak region extending from depths of 50 to 100 nm. This means that even at the lowest fluence used (1 ion/nm^2) spatial overlap of cascades occurs and a large fraction of the atoms in the

TABLE I. Beam parameters and corresponding data extracted from SRIM 2013 and Iradina simulations of Bi irradiated by 400 keV and 1 MeV Au ions. Values of the electronic (Se) and nuclear (Sn) stopping power, projected range (R_p), percentage of transmitted primary ions and recoils, and sputtering yields (Y_s) are given.

	SRIM data							Iradina
E (keV)	S_e (eV/Å)	S_n (eV/Å)	R_p (nm)	Thickness or diameter (nm)	Transmitted primary ions (%)	Transmitted recoils (atoms/ion)	Y_s (atoms/ion)	Y_s (atoms/ion)
400	78	476	65±30	80	30.5	13	20	15,743
				130	3.2	1.8	20	6,874
1000	137	483	129±40	80	81.2	22.5	19	14,020
				130	53.8	19	19	9,746

wire are displaced from their original positions. Recombination, however, is also usually large: for example MD simulations indicate ~90% recovery for defects generated by 500 keV Fe ions in Fe.[25]

The 2D implantation profiles of 400 keV and 1 MeV Au^+ ions into bismuth NWs extracted from Iradina are depicted in Fig. 1. Implantation depth profiles across the center of the wire are also shown, together with the results obtained by SRIM for Bi thin films of thicknesses equal to the wire diameters (Fig. 1b–c). The 1D distributions have similar shapes for the thin films and nanowire, however fewer Au ions end implanted in the nanowire geometry. Naturally, the implanted Au concentration in the NW is even smaller for off-center positions. In the Iradina simulations, the 400 keV Au ions (with a projected range R_p of about 65 nm) are distributed around the center of the 130nm wires (Fig. 1f) or in the bottom half of the 80nm wires (Fig. 1e). For the 1 MeV Au ions (R_p ~130nm), a much lower dopant concentration is observed, distributed mostly near the edge of the wire for both diameters (Fig. 1g and h). Iradina depict more accurately the implantation distribution in a NW, but it still does not take into account changes in the wire shape (due to sputtering and surface diffusion) after each ion impact. The results discussed in the next section, however, indicate that a smooth cylinder geometry for the NW is acceptable up to fluences around 2 ions/nm^2.

Sputtering yields deduced from SRIM for 400 keV and 1 MeV are comparable (around 18-20 atoms/ion, only from the top surface). In a self-supported film there is, in addition, transmitted recoils from the back, with a yield below 25 atoms/ion for both energies (Table I). Hence, the total yield of ejected particles in a planar film geometry predicted by SRIM is below 40 atoms/ion yield. In Iradina, the sputtering yields (atoms exiting all cells around the border of the wire) are much higher, especially at the wire edges (Fig. 1(i)–(l)). For 400 keV Au beam it amounts 15,743 atoms/ion for wires with D_{NW}=80nm and 6,874 atoms/ion for D_{NW}=130 nm. For 1 MeV Au, yields are 14,020 and 9,746 atoms/ion for 80 and 130 nm wires, respectively. These yields correspond to a volume of material equivalent to semi-spherical craters of radii from 6.5 to 4.5 nm. As already pointed out,[12] sputtering in nanowire geometries is substantially enhanced compared to flat surfaces, due to the proximity of the cascades to the wire boundaries and the varied angles of incidence due to the surface curvature. For example, sputtering yields of up to 1900 atoms/ion have been reported from in situ TEM observations of 80 keV Xe ions on Au nanorods.[12]

B. Irradiation effects and wire degradation

Figure 2 shows TEM images of 80 nm diameter Bi nanowires irradiated by 400 keV Au ions at different fluences. Low magnification images depicting the overall evolution of the nanowire's morphology are presented at the left column. The right column shows high resolution micrographs at regions close to the nanowire edges. The as-deposited wires (Figs. 2a–b) are polycrystalline presenting a cylindrical shape and smooth surfaces with tiny corrugations with amplitudes below 2 nm. At low irradiation fluences (Figs. 2c–d), the original crystal structure is preserved at the inner part of the wires. However, there is a change in the TEM contrast at the wire edges indicating significant modification in the original crystal structure and even in the composition. The irradiation also roughened the nanowire surface: at ϕ=1 ion/nm^2 the peak-to-peak roughness amplitude is about 3-5nm. Doubling the fluence, the damaged layer at the edges becomes larger and surface roughening increases (Figs. 2e–f). The wire acquire a wavy appearance with wavelengths of about 40-120 nm and amplitudes of about 5-7 nm.

Figures 2g–i show images of two wires irradiated at a fluence of 10 ions/nm^2. In one case, a section of the nanowire is still continuous, but shows pronounced narrowing and necking, and highly defective regions, with small crystallites and amorphous domains. The other NW is fully broken into spheroidal nanoparticles with diameters close to the original wire. It is noteworthy that the nanoparticles, in this case, present a mean center-to center separation distance of 157 nm, close to $2D_{NW}$. A detailed view of the microstructure of one of these particles is given in Fig. 3. Three distinct layers can be seen: an outer shell of ≈3 nm probably resulting from carbonized residues of the polymeric templates, a polycrystalline 10 nm-thick shell, and a monocrystalline central core. Figure 3d shows a fast-fourier transformation of the lattice image of the inner part of the spheroidal wire segment from Fig. 3c, which provides an interplanar distance correspondent to the Bi (110) lattice planes. While the Bi structure is maintained at the core, the sharp contrast transition between the core and the polycrystalline shell suggests that a change in

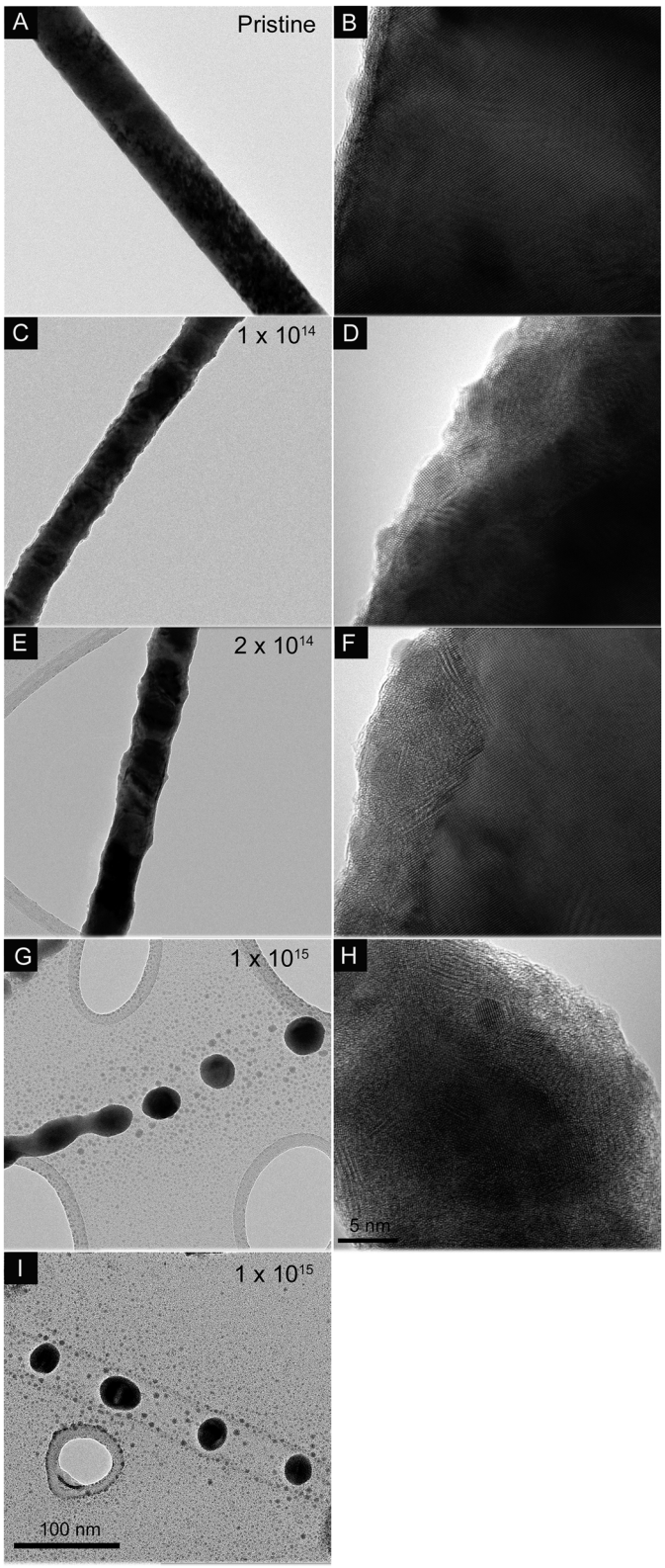

FIG. 2. TEM images of pristine and irradiated 80 nm-diameter bismuth nanowires. Micrographs for a pristine wire are shown in a) and b). NW irradiated by Au 400 keV at fluences of c-d) 1 x 10^{14} e-f) 2 x 10^{14} and g-i) 10^{15} ions/cm^2. The column on the right shows HR-TEM images corresponding to the low magnification images. The scale bar in (i) also apply to images (a, c, e, g). The scale bar in (h) holds for images (b, d, f).

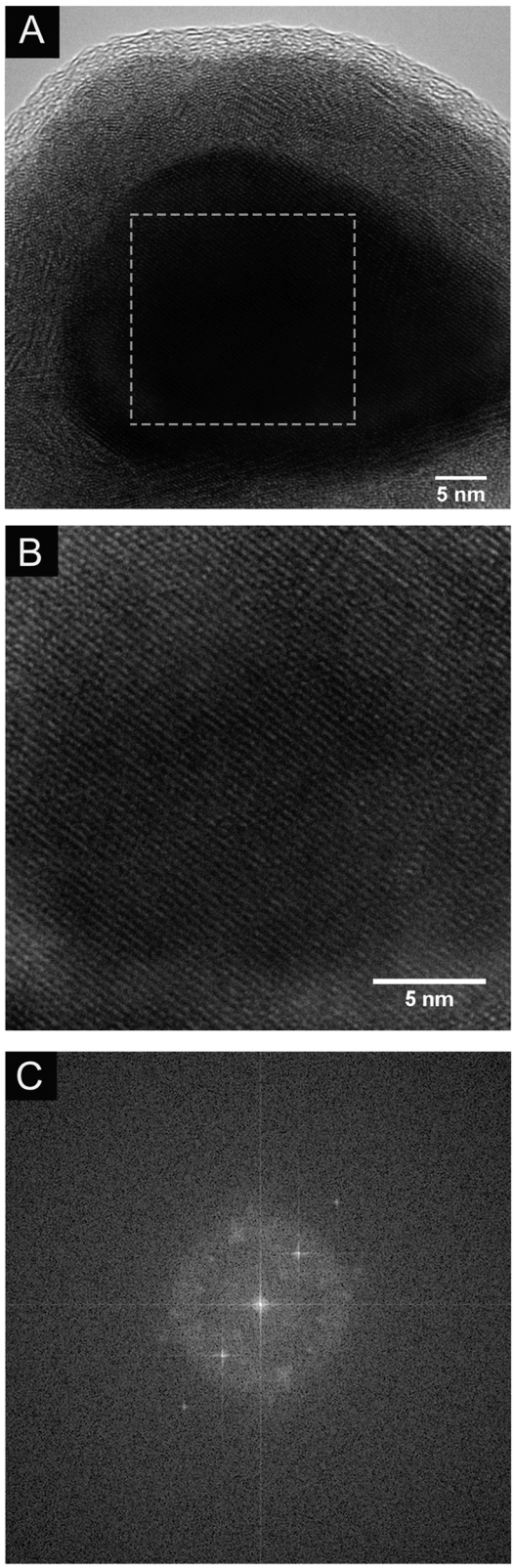

FIG. 3. Microstructure analysis of a nanoparticle from a 80nm-thick degraded nanowire of the type seen in Fig. 2g and 2i. a) HR-TEM image showing the presence of an amorphous outer layer resulting from carbonized residues of the polymeric templates, a polycrystalline shell of bismuth oxide and a monocrystalline Bi central core. b) Zoom from the Bi monocrystalline core of the particle, represented by the dashed white square in a). c) fast-fourier transformation of the region depicted in b).

composition also took place in the shell region. We attribute this to the formation of bismuth oxide, either during the irradiation process or subsequently, due to exposure to the atmosphere before the TEM investigations.

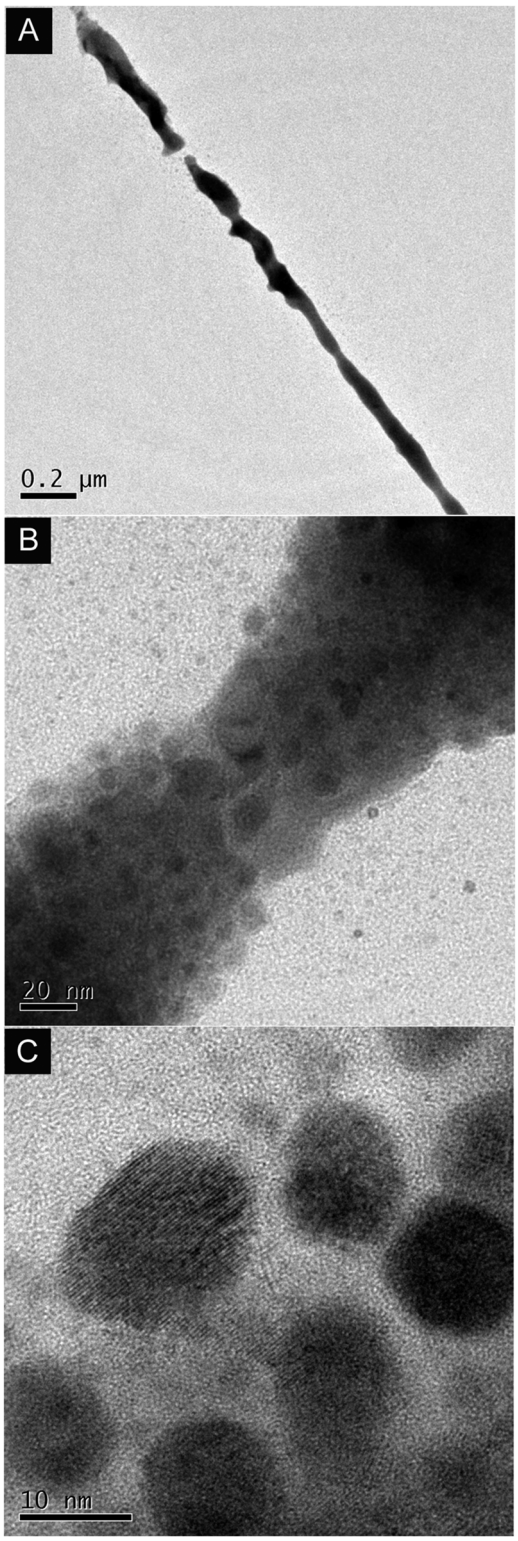

FIG. 4. Bright field TEM images of bismuth nanowires with D_{NW}= 130 nm irradiated by Au 400 keV at 10^{15} ions/cm^2. (a) Low magnification image of a broken wire. The micrographs (b) and (c) show successive zooms on a region with a neck.

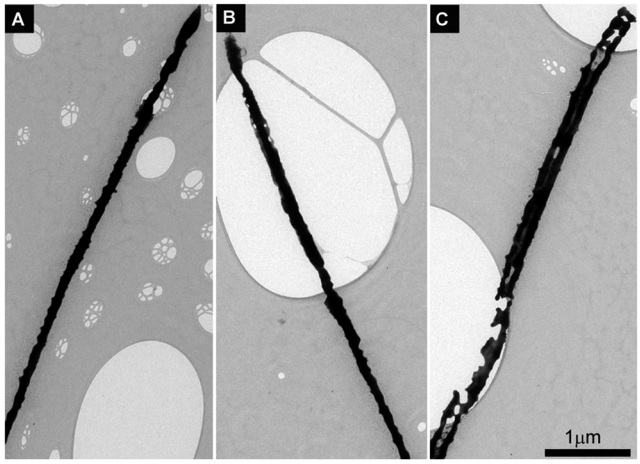

FIG. 5. TEM images of three different Bi nanowires 130 nm in diameter irradiated by Au 1 MeV at 10^{15} ions/cm^2.

Nanowires with diameters of 130 nm were more stable against heavy ion bombardment. Irradiations with 400 keV Au^+ at fluences up to 2 ions/nm^2 do not induce significant modifications in their shapes. However, for a fluence of 10 ions/nm^2 (Fig. 4), the wires roughened substantially and narrowing and necking process are seen. The NW microstructure is characterized by rounded crystalline domains of Bi (with diameters around 10-18 nm) surrounded by amorphous regions most probably composed by bismuth oxide. Although some wires were broken (Fig. 4a), full fragmentation into large spheroidal nanoparticles, as seen for the wires with D_{NW} = 80nm, was not observed. The degradation seen for the 130nm-NWs bombarded by 1 MeV Au ions (Fig. 5) was not very different from that caused by the 400 keV Au beam. However, because of the larger fraction of the wire volume affected by the ions, the erosion tend to be more pronounced. Figure 5c illustrates that in a 130nm-wire irradiated to a fluence of 10 ions/nm^2, where the appearance of holes drilled at the wire center is seen.

It is also clear in the TEM images of NWs bombarded at high fluences (Figs. 2g–i, and Fig. 4b) the presence of a distribution of small nanoparticles, extending to distances of more than 100nm from the original NW boundaries. These particles result most probably from the redeposition of sputtered

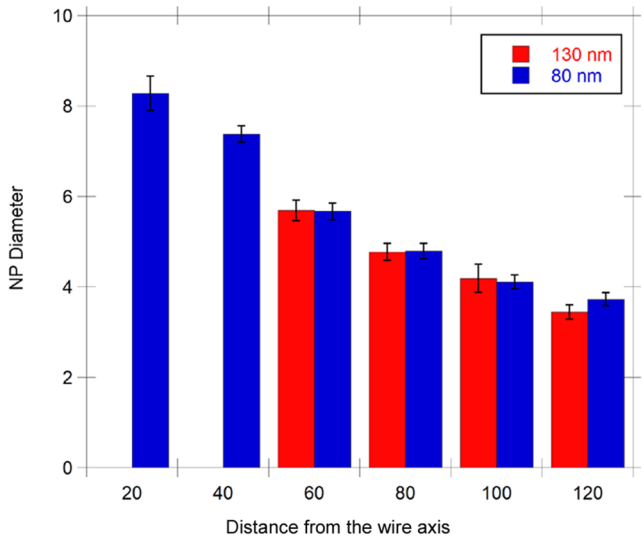

FIG. 6. Mean diameter of nanoparticles surrounding Bi nanowires irradiated by 400 keV Au^+ at 1 x 10^{15} ions/cm^2 as a function of their distance from the central axis of the wires. Data for 80 and 130 nm diameter wires are shown.

Bi atoms or clusters. The particles are polycrystalline and have a size that correlate inversely to their distance from the original wire surface. Figure 6 shows that the average diameter of the nanoparticles decreases from ~8.2 nm close to the wire axis down to ~3.8 nm for particles lying 120 nm from the wire.

IV. DISCUSSION

The overall modifications in shape, structure and composition of the nanowires caused by the Au ion bombardments reflect the intense redistribution of atoms due to dense Bi-Au collision cascades. Sputtering and flow processes induced by the bombardment of keV heavy-ions on flat metal surfaces is well known to cause changes in surface topography like nanometer-sized craters and protrusions.[26] Due to dense collision cascades, a transient thermal-spike can be formed[11,27,28] and ejection of material may occur by either ballistic or evaporative processes. The rapid expansion of the liquid-like zone gives rise also to a pressure pulse which may push out the surface and causes atoms to be explosively ejected.[11,12] This has been observed in simulations of various metal surfaces irradiated by heavy ions[12,29] and should also apply in the present case of 400 and 1000 keV Au ions in Bi. The main difference in the present energy regime is that damage is relatively small at the near surface and peaks only deeper in the solid, after the ion slows down. Yet, the extension of the cascades are comparable to the radii of the NWs and evaporative sputtering might be intense in our case (as compared to e.g., Au nanorods[12]) due to the relatively low melting point of bulk Bi (544 K). As the sputtering yield in nanostructures peaks when there is maximum overlap of the recoil distribution and the nanowires surfaces,[10] the ion energies used in this work, tend to maximize erosion effects, in accordance with the huge yields extracted from the Iradina simulations. This is especially true in the case of 400 keV Au combined with the 80-nm thick nanowires, where, indeed, the most severe damage to the wires was observed in the experiments. For the 130 nm diameter nanowires, morphological changes are more pronounced for the 1 MeV Au beam, which produces cascades on average closer to the bottom of the nanowire, enlarging the overlap with atoms at the near surface and enhancing the probability of particle ejection and surface diffusion processes.

It is not surprising that damage and morphological changes are seen first at the borders of the Bi nanowires (Figs. 2d–e), because sputtering yields are higher at the grazing angles of incidence occurring at the wire edges. With increasing fluence, as the surface roughens and acquires a wavy shape, sputtering is further modified. The local ejection yield is proportional to the surface curvature, which means that more energy is deposited on a surface with a positive curvature (bottom of a valley) than a surface with a negative curvature (top of hills).[10,28] This makes the necks of the NW sputter faster than the bulbous regions, accelerating the breakup of the wire.

Although sputtering plays an important role in the modifications of the NW morphology, the observed surface features are too large to be caused by sputtering only. The energy deposited by the ion creates collective motion of atoms in the cascade core that drives the surface atoms also to diffuse and flow.[30,31] Such local flow processes may amplify the size of topological features on the surface. When atoms moving on surface reach a diffusion barrier,[32] such as grain boundaries, adatoms or surface vacancies across step edges,[22,28] they tend to accumulate creating hills and valleys. These processes depend on the crystallographic directions[28,33] and are usually found on metal surfaces.[22,32,33] It seems worth noting that, even at low temperatures, thermodynamic driving forces such as the minimization of the total interface energy influences atomic flow processes and favors spheroidization and eventually the breakage of the irradiated wires.

Another effect connected to particle flow that can drive surface undulations and break-off of nanoparticles from the wires is the so called end-effect, observed in MC simulations of heated nanowires.[30] The atoms from the ends of the NW tend to form a more bulbous portion than the interior region and a neck is formed. The asymmetry of this end-induced structure drives matter into the wire end, causing neck-narrowing. As the neck narrows, matter is also pulled into the interior of the NW, until its breakage. When a "new end" is formed the process starts again, resulting in the formation of a structure similar to the one seen for the irradiated NW in Fig. 2g. Fragmentation of nanowires into nanoparticles by purely thermal processes has also been associated to the Rayleigh instability[34–36] a process where surface waves are formed and grow on a liquid jet that, causing

its break up into spheres with an average spacing (λ_m). In this model, the correlation between the average spacing and the initial jet radius (r_0) is predicted as $\lambda_m = 9.01\ r_0$.[34,35] However, in our case, the estimated relation between the average spacing and the initial NW radius is $\lambda_m \sim 3.9\ r_0$, which is well below the predicted by Rayleigh instability. Besides, the wavelength of the fluctuations vary among different wires or even within a single wire, as shown in Fig. 2g, while Rayleigh instability is an isometric process. In fact, recent experimental data[33,34] and MC simulations,[30] show that even when the breakage of NW into chains is driven only by thermal processes, it cannot be correctly described by the Rayleigh instability description.

V. CONCLUSION

In conclusion, polycrystalline bismuth nanowires irradiated by 400 keV and 1 MeV Au undergo strong morphological and structural changes, which may lead to full fragmentation into a chain of nanoparticles, depending on the initial wire thickness. For both beams, at fluences of about 10^{15} ions/cm^2 most of the 80nm-thick NWs are decomposed into partially oxidized spheroidal nanoparticles with diameters comparable to the original wire, whilst the thicker wires, although highly eroded, are still unbroken. Besides the morphological changes, the Au ion creates several defects in the bismuth lattice that allow oxygen to interact with the atoms in the edges of the nanowire, enhancing atomic disorder. At lower fluences, these modifications are restricted mostly to the near surface region. At a fluence of 10 ions/nm^2 the oxidation process is more significant and a larger region composed by bismuth oxide is observed, while the Bi structure is maintained either in a distribution of small nanoparticles in the case of the thicker wires or at the core of the spheroidal nanoparticles produced in the highly degraded thin wires. Although several of the observed morphological changes during the process of the wire degradation are similar to those observed in purely thermal decomposition studies, the large sputtering yields and radiation-enhanced flow processes in the nanowires are key to the observed modifications induced by the Au beams.

ACKNOWLEDGMENTS

This work has been partially funded by the research networks of the *National Institute of Surface Engineering* (INCT, CNPq/CAPES) and *Synthesis and Characterization of Nanostructured Materials by Ion Beams* (PRONEX, CNPq/FAPERGS). We also acknowledge GSI for the assistance with the NW templates and Hewlett-Packard Brazil for a scholarship. We are thankful for the discussions with Carsten Ronning and Christian Borschel on Iradina simulations.

[1] T. Shinada, S. Okamoto, T. Kobayashi, and I. Ohdomari, "Enhancing semiconductor device performance using ordered dopant arrays," Nature **437**, 1128–31 (2005).
[2] T. Chang, J. Kim, M.-J. Song, and W. Lee, "Proton irradiation effects on the thermoelectric properties in single-crystalline Bi nanowires," AIP Adv. **5**, 057101 (2015).
[3] Y. Wu, H. Yan, M. Huang, B. Messer, J. H. Song, and P. Yang, "Inorganic semiconductor nanowires: Rational growth, assembly, and novel properties," Chemistry **8**, 1260–1268 (2002).
[4] A. Mavrokefalos, A. L. Moore, M. T. Pettes, L. Shi, W. Wang, and X. Li, "Thermoelectric and structural characterizations of individual electrodeposited bismuth telluride nanowires," J. Appl. Phys. **105**, 104318 (2009).
[5] T. W. Cornelius, M. E. Toimil-Molares, R. Neumann, and S. Karim, "Finite-size effects in the electrical transport properties of single bismuth nanowires," J. Appl. Phys. **100**, 114307 (2006).
[6] D. A. Wright, "Thermoelectric properties of bismuth telluride and its alloys," Nature **181**, 834 (1958).
[7] A. Colli, A. Fasoli, C. Ronning, S. Pisana, S. Piscanec, and A. C. Ferrari, "Ion beam doping of silicon nanowires," Nano Lett. **8**, 2188–93 (2008).
[8] C. Ronning, C. Borschel, S. Geburt, and R. Niepelt, "Ion beam doping of semiconductor nanowires," Mater. Sci. Eng. R Reports **70**, 30–43 (2010).
[9] C. Borschel, M. E. Messing, M. T. Borgström, W. Paschoal, J. Wallentin, S. Kumar, K. Mergenthaler, K. Deppert, C. M. Canali, H. Pettersson, L. Samuelson, and C. Ronning, "A new route toward semiconductor nanospintronics: Highly Mn-doped GaAs nanowires realized by ion-implantation under dynamic annealing conditions," Nano Lett. **11**, 3935–3940 (2011).
[10] A. Johannes, H. Holland-Moritz, and C. Ronning, "Ion beam irradiation of nanostructures: Sputtering, dopant incorporation, and dynamic annealing," Semicond. Sci. Technol. **30**, 033001 (2015).
[11] W. Liu, P. Chen, R. Qiu, M. Khan, J. Liu, M. Hou, and J. Duan, "A molecular dynamics simulation study of irradiation induced defects in gold nanowire," Nucl. Instruments Methods Phys. Res. Sect. B Beam Interact. with Mater. Atoms **405**, 22–30 (2017).

[12] G. Greaves, J. A. Hinks, P. Busby, N. J. Mellors, A. Ilinov, A. Kuronen, K. Nordlund, and S. E. Donnelly, "Enhanced sputtering yields from single-ion impacts on gold nanorods," Phys. Rev. Lett. **111**, 065504 (2013).
[13] Y. Cheng, H. Yao, J. Duan, L. Xu, P. Zhai, S. Lyu, Y. Chen, K. Maaz, D. Mo, Y. Sun, and J. Liu, "Surface modification and damage of MeV-energy heavy ion irradiation on gold nanowires," Nanomaterials **7**, 108 (2017).
[14] A. Johannes, S. Noack, W. Wesch, M. Glaser, A. Lugstein, and C. Ronning, "Anomalous plastic deformation and sputtering of ion irradiated silicon nanowires," Nano Lett. **15**, 3800–3807 (2015).
[15] E. F. Pecora, A. Irrera, S. Boninelli, L. Romano, C. Spinella, and F. Priolo, "Nanoscale amorphization, bending and recrystallization in silicon nanowires," Appl. Phys. A **102**, 13–19 (2010).
[16] L. Romano, N. G. Rudawski, M. R. Holzworth, K. S. Jones, S. G. Choi, and S. T. Picraux, "Nanoscale manipulation of Ge nanowires by ion irradiation," J. Appl. Phys. **106**, 114316 (2009).
[17] J. W. Roh, D. H. Ko, J. Kang, M. K. Lee, J. H. Lee, C. W. Lee, K. H. Lee, J.-S. Noh, and W. Lee, "Proton irradiation effects on thermal transport in individual single-crystalline Bi nanowires," Phys. Status Solidi. **210**, 1438–1441 (2013).
[18] G. Min and D. M. Rowe, "Thermoelectric handbook: Macro to nano," Thermoelectr. Handb. Macro to Nano. 11 (2006).
[19] James Ziegler - SRIM & TRIM, (n.d.). http://www.srim.org/.
[20] Iradina, (n.d.). http://www.iradina.de/ira/index.php?id=download (accessed March 12, 2017).
[21] C. Borschel and C. Ronning, "Ion beam irradiation of nanostructures—A 3D Monte Carlo simulation code," Nucl. Instruments Methods Phys. Res. Sect. B Beam Interact. with Mater. Atoms. **269**, 2133–2138 (2011).
[22] O. Malis, J. D. Brock, R. L. Headrick, M.-S. Yi, and J. M. Pomeroy, "Ion-induced pattern formation on Co surfaces: An x-ray scattering and kinetic Monte Carlo study," Phys. Rev. B **66**, 035408 (2002).
[23] Laboratório de Implantação Iônica - Instituto de Física - UFRGS, (n.d.). https://wiki.if.ufrgs.br/index.php/Laboratório_de_Implantação_Iônica (accessed September 5, 2018).
[24] LabCEMM - Ideia - Centro de Apoio ao Desenvolvimento Científico e Tecnológico, (n.d.). http://www.pucrs.br/ideia/laboratorios/labcemm/ (accessed September 5, 2018).
[25] E. Zarkadoula, S. L. Daraszewicz, D. M. Duffy, M. A. Seaton, I. T. Todorov, K. Nordlund, M. T. Dove, and K. Trachenko, "The nature of high-energy radiation damage in iron," J. Phys. Condens. Matter. **25**, 125402 (2013).
[26] R. C. Birtcher and S. E. Donnelly, "Plastic flow induced by single ion impacts on gold," MRS Proc. **439**, 355 (1996).
[27] C. Dufour, V. Khomenkov, G. Rizza, and M. Toulemonde, "Ion-matter interaction: The three-dimensional version of the thermal spike model. Application to nanoparticle irradiation with swift heavy ions," J. Phys. D. Appl. Phys. **45**, 065302 (2012).
[28] W. L. Chan and E. Chason, "Making waves: Kinetic processes controlling surface evolution during low energy ion sputtering," J. Appl. Phys. **101**, 121301 (2007).
[29] B. Yuan, P. C. Yu, and S. M. Tang, "A database method for binary atomic scattering angle calculation," Nucl. Instruments Methods Phys. Res. Sect. B Beam Interact. with Mater. Atoms **83**, 413–418 (1993).
[30] V. Gorshkov and V. Privman, "Kinetic Monte Carlo model of breakup of nanowires into chains of nanoparticles," J. Appl. Phys. **122**, 204301 (2017).
[31] C.-H. Zhang, F. Kassubek, and C. A. Stafford, "Surface fluctuations and the stability of metal nanowires," Phys. Rev. B **68**, 165414 (2003).
[32] M. Kalff, G. Comsa, and T. Michely, "Temperature dependent morphological evolution of Pt(1 1 1) by ion erosion: Destabilization, phase coexistence and coarsening," Surf. Sci. **486**, 103–135 (2001).
[33] G. Costantini, S. Rusponi, F. B. de Mongeot, C. Boragno, and U. Valbusa, "Periodic structures induced by normal-incidence sputtering on Ag(110) and Ag(001): Flux and temperature dependence," J. Phys. Condens. Matter. **13**, 5875 (2001).
[34] M. E. T. Molares, A. G. Balogh, T. W. Cornelius, R. Neumann, and C. Trautmann, "Fragmentation of nanowires driven by Rayleigh instability," Appl. Phys. Lett. **85**, 5337–5339 (2004).
[35] S. Karim, M. E. Toimil-Molares, A. G. Balogh, W. Ensinger, T. W. Cornelius, E. U. Khan, and R. Neumann, "Morphological evolution of Au nanowires controlled by Rayleigh instability," Nanotechnology **17**, 5954–5959 (2006).
[36] Lord Rayleigh, "On the instability of jets," Proc. London Math. Soc. **s1-10**, 4–13 (1878).